0026-895X/10/7804-588–599$20.00
MOLECULAR PHARMACOLOGY
Vol. 78, No. 4
64014/3623106
Mol Pharmacol 78:588–599, 2010
Printed in U.S.A.

Potassium Channel Block by a Tripartite Complex of Two Cationophilic Ligands and a Potassium Ion[S]

Pavel I. Zimin, Bojan Garic, Silke B. Bodendiek, Cédrick Mahieux, Heike Wulff, and Boris S. Zhorov

Department of Biochemistry and Biomedical Sciences, McMaster University, Hamilton, Ontario, Canada (B.G., B.S.Z.); and Department of Pharmacology, University of California, Davis, California (P.I.Z., S.B.B., C.M., H.W.)

Received February 8, 2010; accepted June 30, 2010

ABSTRACT

Voltage-gated potassium channels (Kv) are targets for drugs of large chemical diversity. Although hydrophobic cations block Kv channels with Hill coefficients of 1, uncharged electron-rich (cationophilic) molecules often display Hill coefficients of 2. The mechanism of the latter block is unknown. Using a combination of computational and experimental approaches, we mapped the receptor for the immunosuppressant PAP-1 (5-(4-phenoxybutoxy)psoralen), a high-affinity blocker of Kv1.3 channels in lymphocytes. Ligand-docking using Monte Carlo minimizations suggested a model in which two cationophilic PAP-1 molecules coordinate a K^+ ion in the pore with their coumarin moieties, whereas the hydrophobic phenoxyalkoxy side chains extend into the intrasubunit interfaces between helices S5 and S6. We tested the model by generating 58 point mutants involving residues in and around the predicted receptor and then determined their biophysical properties and sensitivity to PAP-1 by whole-cell patch-clamp. The model correctly predicted the key PAP-1-sensing residues in the outer helix, the P-loop, and the inner helix and explained the Hill coefficient of 2 by demonstrating that the Kv1.3 pore can accommodate two or even four PAP-1 molecules. The model further explained the voltage-dependence of block by PAP-1 and its thousand-fold selectivity for Kv1.3 over non-Kv1 channels. The 23- to 125-fold selectivity of PAP-1 for Kv1.3 over other Kv1 channels is probably due to its preferential affinity to the C-type inactivated state, in which cessation of K^+ flux stabilizes the tripartite PAP-1:K^+:PAP-1 complex in the pore. Our study provides a new concept for potassium channel block by cationophilic ligands.

Introduction

The pore domain of potassium channels is targeted by drugs of surprisingly different chemical structures. Although the mechanism of action of classic hydrophobic cations such as tetraethylammonium has been intensively studied since the 1960s (Armstrong and Binstock, 1965), much less is known about the mechanism(s) of action of uncharged electron-rich (cationophilic) small-molecule blockers. An example of such blockers is the psoralen derivative PAP-1, which inhibits the voltage-gated Kv1.3 channel in lymphocytes with low nanomolar affinity (IC_{50} 2 nM). The atomistic mechanism of action of PAP-1 and other cationophilic potassium channel blockers is unknown. Understanding this mechanism(s) could potentially aid drug design. Indeed, Kv1.3 and the Ca^{2+}-activated KCa3.1 channels in T-lymphocytes are widely pursued as novel pharmacological targets for immunosuppression (Chandy et al., 2004). Kv1.3 in particular is attractive for autoimmune diseases in which effector memory T cells are involved in the pathogenesis, such as multiple sclerosis, type-1 diabetes mellitus, psoriasis, and rheumatoid arthritis (Beeton et al., 2006). Kv1.3 channels are blocked by

This work was supported by the Natural Sciences and Engineering Research Council of Canada; Canadian Institutes of Health Research [Grant MOP-53229]; the National Institutes of Health National Institute of General Medical Sciences [Grant R01-GM076063]; and a predoctoral fellowship from the Howard Hughes Medical Institutes. The 800 MHz NMR experiments were made possible by the National Science Foundation [Grant DBI722538].

Computations were made possible by the facilities of the Shared Hierarchical Academic Research Computing Network (available at http://www.sharcnet.ca).

B.S.Z. and H.W. are joint senior authors.

Article, publication date, and citation information can be found at http://molpharm.aspetjournals.org.

doi:10.1124/mol.110.064014.

[S] The online version of this article (available at http://molpharm.aspetjournals.org) contains supplemental material.

ABBREVIATIONS: Kv, voltage-gated potassium channel; MC, Monte Carlo; MCM, Monte Carlo minimization; TEA, tetraethylammonium; k, link**e**rs L45; o, **o**uter helix; p, a P-loop; i, **i**nner helix; AS-85, 5-[4-(4-phenoxyphenoxy)butoxy]psoralen; SB4, 1,2-dihydro-*N*-methyl-4-(4-phenoxybutoxy)quinolin-2-one; SB9, 5-(4-phenoxybutoxy)-2*H*-[1]benzopyran-2-one; SB7, 9-(phenoxybutoxy)-9*H*-dibenzo[*b*,*e*]pyran; SB23, 1-(4-phenoxybutoxy)anthraquinone; SB24, 9-(4-phenoxybutoxy)phenanthrene; PAP-1, 5-(4-phenoxybutoxy)psoralen; PAPS, 4-(4-phenoxybutoxy)-7*H*-furo[3,2-*g*]chromene-7-thione; MK-499, (+)-*N*-[1′ (6-cyano-1,2,3,4-tetrahydro-2(*R*)-naphthalenyl)-3,4-dihydro-4(*R*)-hydroxyspiro(2*H*-1-benzopyran-2,4′-piperidin)-6-yl]methanesulfonamide] monohydrochloride; TRAM-34, 1-[(2-chlorophenyl)diphenylmethyl]-1*H*-pyrazole.

peptide toxins and small-molecule ligands. In the absence of an X-ray structure of Kv1.3 with a bound small-molecule ligand, structure-based drug design is not feasible, and all existing small-molecule Kv1.3 blockers have been identified either through the extraction of medicinal plants or high-throughput screening followed by medicinal chemistry optimization (Wulff and Pennington, 2007; Wulff and Zhorov, 2008). Mapping the receptor sites for such blockers is an important and challenging goal on the long road toward designing potent and safe small-molecule Kv1.3 blockers for immunosuppression.

The pore-forming domain of Kv1.3 is believed to fold like Kv1.2, whose open-state X-ray structure shows four subunits circumferentially arranged around the central pore (Long et al., 2005). Each subunit has six transmembrane helices S1 to S6, and a membrane reentering extracellular P-loop. Four voltage-sensing domains, each formed of S1 to S4, are connected via the linking helices L45 to the pore domain formed of S5s, S6s, and the P-loops. The inner pore of K^+ channels is a major target for small-molecule blockers (Wulff and Zhorov, 2008), and the mechanism of block by internally applied quaternary ammonium ions is well understood (Armstrong, 1971; del Camino et al., 2000). Crystallographic studies have provided several structures of the bacterial KcsA channel blocked by tetra-alkylammonium compounds (Zhou et al., 2001a; Lenaeus et al., 2005; Faraldo-Gómez et al., 2007), in which the ammonium group occurs at the pore axis close to the focus of the P-loop helices. In the ligand-free channel, this position is occupied by a K^+ ion (Zhou et al., 2001a). Tetra-alkylammonium compounds and other hydrophobic cations, such as the L-type Ca^{2+} channel blocker verapamil, also block the inner pore of Kv1.3 (Rauer and Grissmer, 1996; Dreker and Grissmer, 2005) but lack Kv1.3-specificity and therefore are not useful as immunosuppressants. Another class of Kv1.3 blockers is psoralens, which were initially extracted from the rue plant *Ruta graveolens* (Vennekamp et al., 2004). The most potent psoralen, PAP-1, blocks Kv1.3 at low nanomolar concentrations and, according to electrophysiological experiments, preferentially inhibits the C-type inactivated state of the channel (Schmitz et al., 2005). PAP-1 is currently in early preclinical development for psoriasis because it has been demonstrated to treat allergic contact dermatitis (Azam et al., 2007), an animal model for psoriasis. PAP-1 has further been shown to prevent type-1 diabetes development in rats (Beeton et al., 2006).

The structure of PAP-1 differs markedly from that of hydrophobic cations such as tetraethylammonium or verapamil. Although the organic cations block Kv channels with a Hill coefficient close to unity, the uncharged lipophilic PAP-1 inhibits Kv1.3 with a Hill coefficient of 2 (Schmitz et al., 2005), suggesting that two or more ligands bind simultaneously. Uncharged compounds that block cation channels with Hill coefficients of more than one are not uncommon. Other examples are *S*-nitrosodithiothreitol as a general Kv1 family channel blocker (Brock et al., 2001), disubstituted cyclohexyl analogs as Kv1.3 blockers (Schmalhofer et al., 2002), and benzocaine as a Na^+ channel blocker (Meeder and Ulbricht, 1987). All of these compounds have electron-rich groups and few (if any) H-bond donors. Given their overall electroneutrality, these molecules could interact favorably with organic or inorganic cations. Earlier we hypothesized that such cationophilic molecules chelate a metal ion at the focus of the P-loop helices with a 2:1 stoichiometry and thus potentially occupy the same region in the inner pore as hydrophobic cations (Tikhonov et al., 2006). Below we describe experiments that support the hypothesis that a K^+ ion also forms an important part of the PAP-1 binding site and demonstrate that this high-affinity Kv1.3 blocker binds to the inner pore and extends its flexible side chain into the intra-subunit interfaces between helices S5 and S6.

Materials and Methods

Homology Modeling of Kv1.3 and PAP-1 Docking. The amino acid sequence of the human Kv1.3 channel (KCNA3_HUMAN; UniProtKB/Swiss-Prot P22001) was used to build the model of the pore domain. The conformational energy expression included van der Waals, electrostatic, H-bonding, hydration, and torsional components, as well as energy of deformation of bond angles in ligands. All bond lengths and bond angles in the protein were kept rigid. Nonbonded interactions were calculated using the AMBER force field (Weiner et al., 1984, 1986). Electrostatic energy was calculated with the distance-dependent dielectric function $\varepsilon = r$, where r is the distance between a pair of interacting atoms. The hydration energy was calculated using the implicit-solvent method (Lazaridis and Karplus, 1999). Atomic charges for the PAP-1 molecule were calculated using the AM1 method (Dewar et al., 1985) realized in MOPAC (available at http://openmopac.net/home.html).

All ionizable residues were modeled in the neutral form (Lazaridis and Karplus, 1999). Nonbonded interactions were truncated at distances >8 Å. This cutoff distance allows to speed up calculations without a noticeable precision decrease of energy calculations (Bruhova and Zhorov, 2007). The energy was minimized in the space of generalized coordinates, which include all torsion angles, bond angles of the ligand, positions (Cartesian coordinates) of ions, positions of root atoms of the ligands and protein subunits, and orientations (Euler angles) of triplets of atoms that include the root atoms and two of its valence neighbors (Zhorov, 1981, 1983).

The starting backbone geometry was assigned from the Kv1.2 template. All-*trans* conformations were used as starting approximations for the side chains of residues, which are not defined in the X-ray structure of Kv1.2 or mismatch between Kv1.3 and Kv1.2. For other residues, the starting conformations of side chains were taken from the Kv1.2 template. The α-carbons were constrained to matching positions in the Kv1.2 template with the help of pins. A pin is a flat-bottomed penalty function (Brooks et al., 1985) that allows a penalty-free deviation of the respective atom up to 1 Å from the template and imposes an energy penalty for larger deviations. Similar flat-bottomed constraints were used to bias the coordination of the potassium ion at position 5 (K^+_{T5}) to carbonyl oxygens of two PAP-1 ligands and to prevent large deviations of K^+_{T5} from the pore axis. The force constant of 10 kcal · mol^{-1} · $Å^{-1}$ was used in the constraints.

At the seeding stage, the energy of a starting point was optimized using the multistep relaxation with Monte Carlo minimizations (MCMs). First, all generalized coordinates (degrees of freedom) of the starting structure were frozen, except for those that govern the positions and orientations of the ligands and the position of K^+_{T5}. All interactions were switched off, and the constraints energy was minimized in a short MCM trajectory (10 minimizations) to bring the carbonyl oxygens of the PAP-1 ligands to K^+_{T5} without allowing K^+_{T5} to deviate significantly from the pore axis. Then all interactions were switched on, and the energy was optimized in five consecutive MCM trajectories (10 minimizations in each trajectory) with stepwise unfreezing of the following degrees of freedom: 1) torsions angles of the ligands, positions of K^+ ions, and positions and orientations of water molecules in the selectivity filter; 2) side chain torsions of the protein; 3) the protein main chains torsions; and 4) degrees of freedom that govern positions and orientations of the channel subunits. At

stages 3 and 4, pin constraints were used to prevent any significant deviations of the protein backbones from the X-ray template. At the refinements stage, the energy was MC-minimized without any constraints. All calculations were performed using the ZMM program (available at http://www.zmmsoft.com).

Mutant Channel Constructs. Human Kv1.3/pRC/CMV (GenBank accession number L23499) was a generous gift from Dr. Carol Deutsch (University of Pennsylvania, Philadelphia, PA). Mutations were introduced using the QuikChange mutagenesis kit (Stratagene, La Jolla, CA) and were verified by fluorescence sequencing.

Transfection. L-929 cells (American Type Culture Collection, Manassas, VA) were cultured in Dulbecco's modified Eagle's medium supplemented with 10% fetal bovine serum, 1 mM sodium pyruvate, 100 U/ml penicillin, and 100 μg/ml streptomycin. Cells were transfected with FuGENE6 Transfection Reagent in Opti-MEM medium according to the manufacturer's protocol and analyzed typically within 12 to 48 h after transfection. Kv1.3 DNA was cotransfected with eGVP-C1 to enable the visualization of transfected cells.

Patch-Clamp Experiments. Patch-clamp experiments were carried out at room temperature in the whole-cell configuration using an EPC-10 amplifier (HEKA, Bellmore NY). The external solution contained 160 mM NaCl, 4.5 mM KCl, 2 mM $CaCl_2$, 1 mM $MgCl_2$, and 10 mM HEPES, pH 7.4, with osmolality of 300 mmol/kg. The internal pipette solution contained 160 mM KF, 2 mM $MgCl_2$, 10 mM HEPES, and 10 mM EGTA, pH 7.2, with osmolality of 300 mmol/kg. Pipette resistance was between 1.5 and 3 MΩ. The holding potential was -80 or -100 mV in most cases but was lowered (between -110 and -170 mV) for mutants that showed incomplete fractional recovery. These changes in recovery might of course suggest that the mutations somewhat affected inactivation. However, because the mutations did not significantly change inactivation time constants and use-dependence (both crucial parameters influencing PAP-1 activity), we decided to include these mutants in our study and adjusted the holding potential until no steady-state inactivation was observed. Series resistance compensation (80%) was used for currents larger than 2 nA. All curve-fittings were performed using Origin 7 software (OriginLab Corp, Northampton, MA).

The conductance-voltage relationship was determined by stepping from the holding potential to different depolarizing levels up to +80 mV in 10-mV increments. In cases in which conductance did not saturate, tail currents were used to measure half-voltage activation. Cells were depolarized for 40 ms to voltages ranging from -80 to +60 mV in 10-mV increments followed by the tail current measurement at -40 mV. Peak currents were fitted with the Boltzmann function to calculate the half-activation voltage ($V_{1/2}$). Activation and inactivation time constants were calculated by fitting current traces obtained after depolarization steps to +40 mV with a modified Hodgkin-Huxley type n^4j kinetics model [$I_{total} = I_c(1 - \exp(-t/\tau_n))^4\exp(-t/\tau_h + D)$] , where I_{total} is total current, I is current parameter, exp is exponential function, t is time in seconds, τ_n is the activation time constant, τ_h is the inactivation time constant, and D is the steady state component. The Normalized steady-state current R was calculated by extrapolating current to infinity and dividing it by the peak current ($R = I_\infty/I_{peak}$). Cumulative inactivation was characterized by 10 repetitive 200-ms depolarizing pulses from the holding potential to +40 mV every second. The ratio between the charge (area under the curve) of the fifth pulse and the charge of the first pulse was used as a parameter to characterize cumulative inactivation. Statistically significant changes of τ_h, R, and cumulative inactivation were assessed with 2-tailed unpaired Student's t test. To measure IC_{50} values for PAP-1, currents were elicited by 500-ms depolarizing pulses from the respective holding potential to +40 mV. The normalized residual peak current ($I_{PAP\text{-}1}/I_{control}$) after obtaining equilibrium block was used to generate dose-response curves. Because the potency of PAP-1 potency depends on the holding potential (Fig. 1 and Supplementary Table 2), significance for changes in PAP-1 potencies were assessed by comparing the normalized residual current from each mutant with the wild-type channel held at the corresponding holding potential with two-tailed unpaired Student's t test.

Results

PAP-1 Competes with the Pore Blockers TEA and Verapamil. Kv1.3 can be identified biophysically by its characteristic C-type inactivation and its pronounced cumulative inactivation after repeated depolarizing pulses (Cahalan et al., 1985; Panyi et al., 1995). We reported previously that PAP-1 shows preference for the C-type inactivated state of Kv1.3 based on experiments varying the pulse lengths, the extracellular K^+ concentration, and the activation state of the channel through repetitive pulsing (Schmitz et al., 2005). State-dependent channel inhibition like this can theoretically be achieved by ligands binding to various channel domains including the pore, the voltage-sensor domains, and the N or C termini. To determine whether PAP-1 blocks the

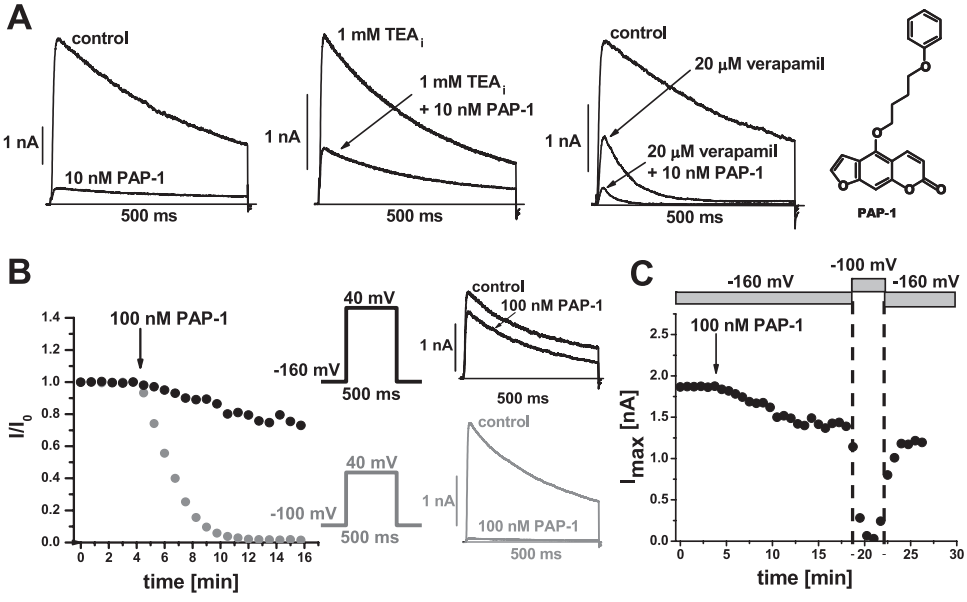

Fig. 1. PAP-1 competes with inner pore blockers and shows voltage-dependent blockade of Kv1.3. A, PAP-1 competition with internal TEA and external verapamil. Current traces were recorded in the absence or presence of 10 nM PAP-1 either alone or in combination with 1 mM internal TEA or 20 μM external verapamil. B, block of Kv1.3 current at 40 mV by 100 nM PAP-1 with holding potentials of -100 and -160 mV (500-ms pulse applied every 45 s). C, on switching the holding potential from -160 to -100 mV, PAP-1 block rapidly develops and then reverses again (same pulse protocol as in B).

inner pore, we performed competition experiments with the known Kv1.3 inner-pore blockers TEA_i and verapamil (Rauer and Grissmer, 1996; Dreker and Grissmer, 2005). If two compounds act at independent sites, their effects are additive, and a fixed concentration of PAP-1 would achieve the same percentage of inhibition irrespective of whether the other compound is present or not. In contrast, if PAP-1 and the other compound act at the same or overlapping binding sites, the percentage of current inhibition by PAP-1 should be smaller than when PAP-1 is applied alone. In a whole-cell experiment, 10 nM PAP-1 achieved 92 ± 9% block at steady state (Fig. 1A, left; $n = 3$). However, when PAP-1 was applied into the bath with 1 mM TEA present in the pipette, which inhibits Kv1.3 on the internal TEA site with an IC_{50} of 0.6 mM (Aiyar et al., 1994), PAP-1 only achieved 65 ± 7% block at steady state (Fig. 1A, middle; $n = 3$). In another experiment, we first applied 20 μM verapamil into the bath and then perfused 20 μM verapamil plus 10 nM PAP-1 and found that PAP-1 inhibited the current remaining after verapamil block by only 74 ± 3% (Fig. 1A, right; $n = 3$). Taken together, the results of these experiments indicate that PAP-1 competes with TEA_i and verapamil and therefore blocks the inner pore of Kv1.3.

Kv1.3 Block by PAP-1 Is Voltage-Dependent. All of our experiments published previously with PAP-1 had been performed with a holding potential of −80 mV. Here we depolarized the membrane to 40 mV from a holding potential of −100 mV for 500 ms at 45-s intervals and found that 100 nM PAP-1 completely blocked the current (Fig. 1B), in agreement with the published IC_{50} of 2 nM determined at a holding potential of −80 mV (Schmitz et al., 2005). In contrast, when we performed the same experiment at a holding potential of −160 mV, the same PAP-1 concentration only blocked 20% of the current (Fig. 1B). When we then changed the holding potential on the same cell back to −100 mV, we again observed nearly complete block on the next depolarizing pulse 45 s later. This block could be relieved by returning the holding potential to −160 mV (Fig. 1C). There are at least two possible explanations for this experiment. First, the strongly hyperpolarizing holding potential distorts the channel structure and thus reduces PAP-1 potency. However, this scenario is unlikely because the biophysical properties of Kv1.3 at −100 and −160 mV are not significantly different in terms of $V_{1/2}$, activation and inactivation time constants (Supplementary Table S1), and recovery from inactivation (Fig. 2). The second possibility is that the PAP-1 molecules move with the electrical field. Because PAP-1 is uncharged and contains no protonatable groups, the simplest explanation for our observations is that not the PAP-1 molecules per se but their complexes with K^+ sense the voltage changes.

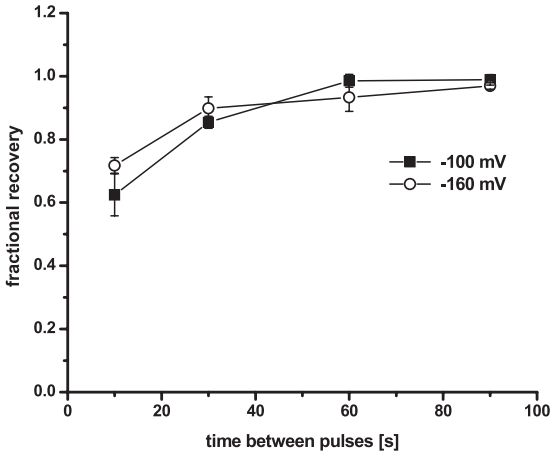

Fig. 2. The time courses of wild-type Kv1.3 recovery are indistinguishable from each other at holding potentials of −100 and −160 mV. A two-pulse protocol was used in which two depolarizing pulses to +40 mV with a duration of 500 ms were separated by 10, 30, 60, and 90 s. The peak current of the second pulse was divided by the peak current of the first pulse, and the ratio was plotted.

Structure-Activity Relationships of PAP-1 Analogs. Growing computational evidence suggests that uncharged lipophilic ligands, which target the pore region of cationic channels, may directly interact with permeating ions in the channel pore. This concept allowed us to recently propose structural models that explain long-known effects of metal ions on L-type Ca^{2+} channel ligands (Tikhonov and Zhorov, 2008; Cheng et al., 2009; Tikhonov and Zhorov, 2009). We also explained previously the observations that the cationic lidocaine and the uncharged benzocaine block Na^+ channels with Hill coefficients of 1 and 2, respectively, by a model in which two benzocaine molecules coordinate an Na^+ ion in the permeation pathway (Tikhonov et al., 2006). Based on the above-described experiments and the fact that the uncharged PAP-1 inhibits Kv1.3 with a Hill coefficient of 2 (Schmitz et al., 2005), we hypothesized that Kv1.3 is blocked by a tripartite complex consisting of two PAP-1 molecules and a K^+ ion.

PAP-1 has five oxygen atoms (Fig. 3), each of which can attract a K^+ ion. To define the oxygen atoms involved in K^+ coordination, we synthesized 27 PAP-1 analogs in which the oxygens were either removed or substituted with other heteroatoms (Bodendiek et al., 2009). A selection of these compounds is shown in Fig. 3 to illustrate the most intriguing features of the structure-activity relationship. Removal of the furan ring [5-(4-phenoxybutoxy)-2*H*-[1]benzopyran-2-one (compound SB9)] was relatively well tolerated and only reduced activity by 75-fold,

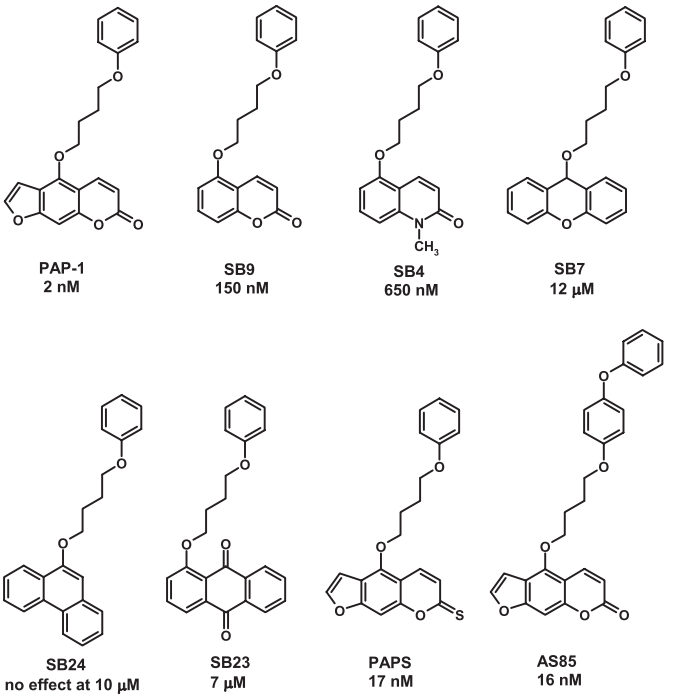

Fig. 3. Structures and IC_{50} values for PAP-1 and selected derivatives.

whereas removing or shifting the coumarin carbonyl resulted in a more than 1000-fold reduction in activity or in a complete loss of potency [9-(phenoxybutoxy)-9*H*-dibenzo[*b*,*e*]pyran (SB7), 9-(4-phenoxybutoxy)phenanthrene (SB24), and 1-(4-phenoxybutoxy)anthraquinone (SB23)]. Submicromolar activity further required a planar bi- or tricyclic aromatic ring system. These experiments suggested a key role of the coumarin carbonyl oxygen for the Kv1.3 blocking activity of PAP-1. This oxygen should have an electron-deficient counterpart in the PAP-1 receptor, which could be a basic group, an H-bond donor, or a K^+ ion. The first possibility can be eliminated because the inner pore of Kv1.3 lacks basic residues. To choose between the latter two possibilities, we synthesized a compound, 4-(4-phenoxybutoxy)-7*H*-furo[3,2-*g*]chromene-7-thione (PAPS), in which the carbonyl oxygen was replaced by a sulfur atom, and found that it blocked Kv1.3 with an IC_{50} of 17 nM (Fig. 3). Because sulfur is a very poor H-bond acceptor (Zhou et al., 2009) but readily coordinates a K^+ ion with a sulfur-to-K^+ distance of 3.2 to 3.3 Å (Hazel and Collin, 1972; Sieler et al., 1985), which is just 0.3 Å longer than the oxygen-to-K^+ distance, these data strongly support the idea that the PAP-1 carbonyl oxygen does not act as a hydrogen bond acceptor. Taken together, the structure-activity relationships of the PAP-1 analogs are best explained by a direct interaction of the cationophilic PAP-1 with a K^+ ion. Using 800-MHz NMR spectroscopy, we observed a 0.02 ppm shift in the ^{13}C signal of the carbonyl carbon atom (C2) and the conjugated C4 on addition of potassium perchlorate (Supplementary Table S2), suggesting a change in hybridization for these two atoms indicative of the formation of a weak complex between PAP-1 and K^+.

Molecular Model of the PAP-1 Binding Site. In the absence of a crystal structure of Kv1.3, we have built a homology model based on the X-ray structure of the open Kv1.2 channel (Long et al., 2005). The voltage-sensing and cytoplasmic domains that are far from the known binding region of TEA_i and verapamil, which compete with PAP-1, were not included in the model. The model consists of the four channel subunits: two PAP-1 molecules, K^+ ions in positions 1, 3, and 5, and explicit water molecules in positions 2 and 4 of the selectivity filter. Because an unbiased computational prediction of the global-minimum complex of the channel protein with two flexible ligands and a K^+ ion is hardly possible (see below), we docked the PAP-1:K^+:PAP-1 complex using three distance constrains implied by our structure-activity studies. The carbonyl oxygens of two PAP-1 ligands were constrained within 3 Å from a K^+ ion at position 5 and the K^+ ion was constrained within 2 Å from the pore axis.

The Kv1.3 model and its complexes with ions and ligands were then optimized using the MCM method (Li and Scheraga, 1987) realized in the ZMM program (Zhorov, 1981; Garden and Zhorov, 2010). The energy hypersurface of a complex molecular system has an extremely ragged shape. A single MCM trajectory can sample only a small part of such a surface. Therefore, we searched energetically optimal complexes by a two-stage approach. At the seeding stage, 40,000 MCM trajectories were submitted from different starting points (Bruhova and Zhorov, 2007; Tikhonov and Zhorov, 2007). A starting point was generated with random positions, orientations, and conformations of the two ligands. In the randomly sampled structure, the ligands initially overlapped with the protein in multiple places, resulting in an unrealistically high starting energy. This energy was optimized using the stepwise MCM relaxation procedure described under *Materials and Methods*. To reduce the number of collected structures, geometrically similar complexes were clustered and represented by their lowest energy structures. The above seeding stage was not expected to yield realistic structures, but it provided energy estimates to discard unpromising complexes with energies >1000 kcal/mol from the apparent global minimum found at this stage. At the second, refining stage, each complex collected at the seeding stage was further optimized in an MCM trajectory of 1000 minimizations with sampling of all torsions in the ligands and the protein as well as positions and orientations of the ligands. Geometrically similar structures found in the refining stage were clustered. Structures within 7 kcal/mol from the apparent global minimum were analyzed.

In the apparent global minimum and in several local minima, one of the two PAP-1 ligands had a position close to that shown in Fig. 4, whereas the phenylalkyl moiety of the second PAP-1 ligand was found in various positions (data not shown). The ligand-channel energy for the first ligand was lower than that for the second ligand. The inability of the docking protocol to predict a complex with two PAP-1 ligands symmetrically bound is not surprising in view of the very large number of local minima in the flexible system and the limited converging space of individual MCM trajectories. We then used distance constraints to place the second PAP-1 ligand into a position symmetrical to the first ligand, Monte Carlo-minimized this structure, and arrived at a complex with a lower energy than the best structure found "hands-free." Finally, we removed all constraints and Monte Carlo-minimized the complex until the energy of the apparent global minimum did not decrease during 2000 consecutive MCM steps. This complex (Fig. 4 and a movie in the Supplementary material) was used to guide the mutational analysis of the PAP-1 binding site.

In the predicted complex, the coumarin moieties of two ligands interact with the P-loop turn and S6s, whereas the long flexible arms protrude into the intrasubunit interfaces between S6s and S5s and approach linkers L45 (Fig. 4B). To describe the binding site, we designate residues by the subunit number (in the extracellular view, subunits 1 to 4 are arranged clockwise), segment index ("*k*" for linkers L45, "*o*" for outer helices, "*p*" for P-loops, and "*i*" for inner helices), and the residue number within the segment (Fig. 4A). The predicted binding site for each PAP-1 molecule (Fig. 4, B–E) contains four loci of residues whose side chains have at least one heavy atom within 5 Å from the ligand (Fig. 4, D and E, and Supplemental Table S3). Locus I is the inner pore, a common binding region for K^+ channel ligands (Sanguinetti and Tristani-Firouzi, 2006; Wulff and Zhorov, 2008). It accommodates the K^+-bound carbonyl groups and parts of the coumarin moieties from both PAP-1 molecules. Locus II between two neighboring S6s (immediately below the gating-hinge G^{i14}) accommodates the benzofuran ring and adjacent to it part of the butoxy chain. Locus III between helices S5 and S6 of the same subunit accommodates the remaining part of the butoxy chain. Locus IV, which involves L45 and S6 of one subunit and S5 and S6 of the neighboring subunit, accommodates the PAP-1 phenyl ring. The two PAP-1 ligands bind at the opposite sides of the pore with their coumarin moieties approximately in the same plane (Fig. 4C). Approx-

imate locations of the PAP-1 binding loci are shown in Supplemental Fig. S1. Energy contributions of the channel residues and PAP-1 atoms to the binding energy are shown in Supplemental Tables S3 and S4. None of the channel residues provides a positive (repulsive) energy contribution of >0.2 kcal/mol, and none of the ligand atoms provides a positive contribution of >0.16 kcal/mol. Phenylalanine F^{o13} provides the largest side-chain contribution to PAP-1 binding energy (−3.02 kcal/mol) due to π–π stacking interactions with the aromatic ring of PAP-1 (Fig. 4, D and E).

PAP-1 Molecules Chelate the K^+ Ion and Interact with Its Solvation Shell. Figure 4 shows that two PAP-1 molecules contribute two carbonyl oxygens to the first solvation shell of the K^+ ion in the central cavity. The ether oxygens in the PAP-1 coumarin rings are ~4.5 Å from the K^+ ion, which is too far for them to contribute to the first solvation shell. According to the implicit-solvent model (Lazaridis and Karplus, 1999), these vacancies in the solvation shell are filled by water molecules. Is our model consistent with experimental data on K^+ coordination geometry? The high-resolution X-ray structure of the KcsA-FAB complex shows eight ordered water molecules, which coordinate a K^+ ion in the cavity center of the channel (Zhou et al., 2001b). The idealized geometric equivalent of this structure is a square antiprism in which the K^+ ion occupies the center, the oxygen atoms of the water molecules are in the vertices of the rectangular planes, which are normal to the pore axis, and the rectangle proximal to the selectivity filter is rotated 45° around the pore axis with respect to the rectangle distant from it. To explore possible coordination geometries of the K^+ ion bound to two PAP-1 ligands in Kv1.3, we added six water molecules to our model and used flat-bottomed penalty functions (see *Materials and Methods*) to constrain the distances between the water oxygens and the K^+ ion within 2 to 5 Å. The number of water molecules and the upper distance limit was chosen to bias toward the presence of up to eight oxygen atoms on the coordination sphere but not toward any specific coordination geometry. The starting coordinates of the water molecules within the cavity were randomly generated to rule out any bias toward the experimental structure. At the first stage, the energy was Monte Carlo-minimized in the space of 36 degrees of freedom that govern positions and orientations

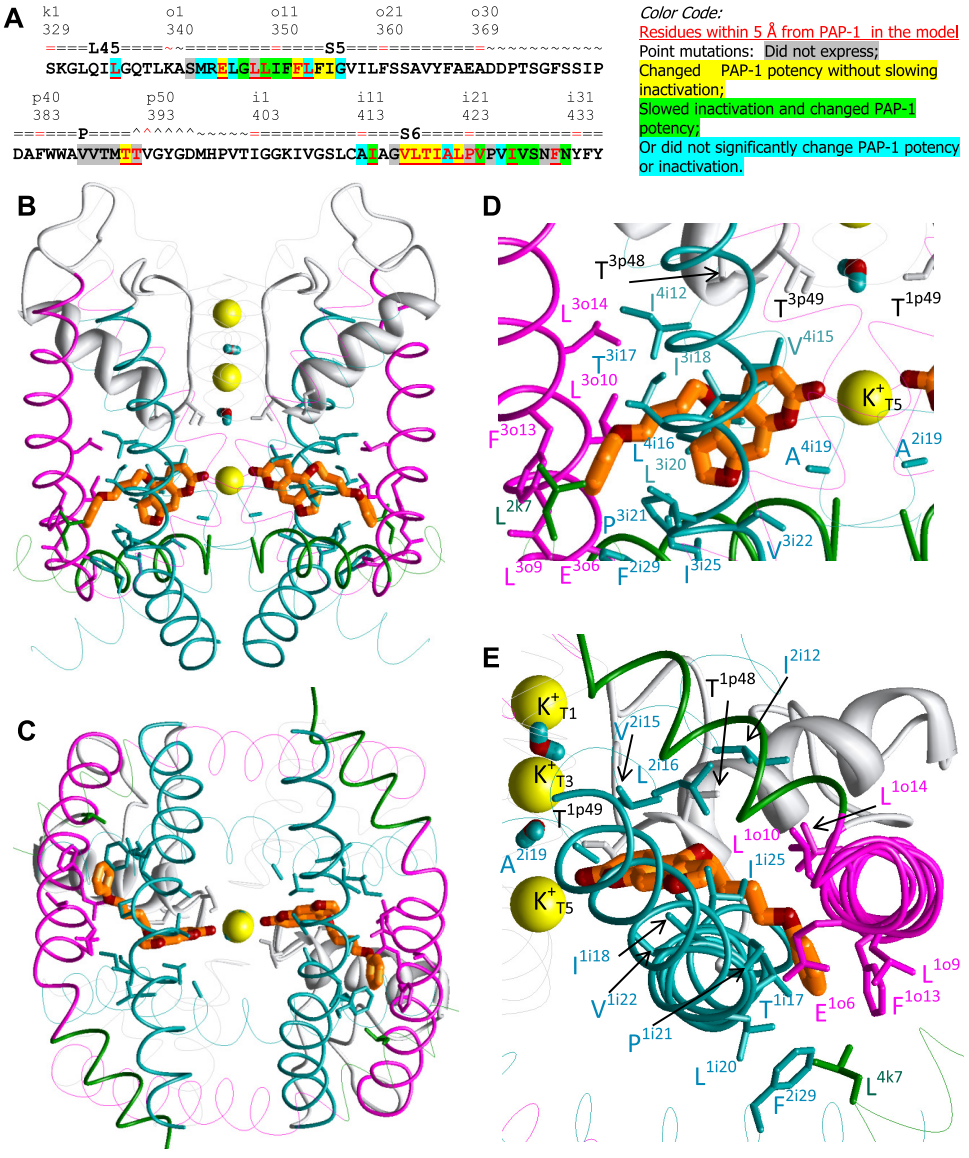

Fig. 4. Block of Kv1.3 by the tripartite complex PAP-1:K^+:PAP-1. A, human Kv1.3 pore domain sequence and summary of the mutational, biophysical, and PAP-1 blocking experiments. Special symbols mark helices (=), loops/turns (~), and the selectivity-filter region (^). Residue labels and numbers are shown above the respective residues. A label consists of a segment-encoding character and the relative number of the residue in the segment. Character **k** stands for a lin**k**er L45, **o** for an **o**uter helix (S5), **p** for a **P**-loop, and **i** for an **i**nner helix (S6). B and C, side and cytoplasmic views of the tripartite complex in Kv1.3. Sites 1 to 5 in the permeation pathway are occupied by three K^+ ions (yellow spheres) and two water molecules. Helices L45, S5, and S6 are shown as green, magenta, and cyan rods, respectively. P-helices are gray ribbons. P-turns, ascending limbs, and extracellular loops are shown as gray rods. PAP-1 molecules are shown with red oxygens and orange carbons. Side chains within 5 Å from PAP-1 molecules are shown as sticks. For clarity, backbones in subunits 2 and 4 are shown as wire frames. D, enlarged side view at PAP-1 bound between 2L45, 2S6, 3S5, 3P, 3S6, and 4S6. E, enlarged view from the C-end of 1S6 along the helix axis at PAP-1 bound between 1S5, 1P, 1S6, 2S6, 4L45, and 4S6.

of the six water molecules. The system was then Monte Carlo-minimized without the distance constraints and with all degrees of freedom relaxed. In the resulting structure (Fig. 5, A and B), the predicted coordination geometry of the K^+ ion in the cavity center is similar to that in the X-ray structure (Zhou et al., 2001b). The vertices of the square-antiprism rectangle, which is proximal to the selectivity filter, contain the carbonyl oxygens of two PAP-1 molecules and two water molecules. The lower rectangle, which is rotated ~45° around the pore axis in respect to the upper one, contains four water molecules, which donate four H-bonds to the ether oxygens of the two PAP-1 molecules. These results suggest that the ether oxygens are very important for PAP-1 activity and explain why compound SB9 (Fig. 3) is ~4.5 times more active than its analog 1,2-dihydro-*N*-methyl-4-(4-phenoxybutoxy)quinolin-2-one (SB4) (Bodendiek et al., 2009), in which the ether oxygen is replaced by an N-CH_3 group (Fig. 3). The oxygen atoms in the upper rectangle are 5.4 to 6.3 Å from the closest side-chain oxygen atoms ($O^{\gamma 1}$ in T^{p49}) and can be linked to the latter atoms via single-water bridges, as suggested by the KcsA structure (Zhou et al., 2001b). It should be noted that the explicit water molecules practically did not shift the tripartite complex from the position predicted with the implicit-solvent approach (Fig. 4). Although no constraints were imposed during the refinement MC minimization with the implicit solvent, the two carbonyl oxygens of the PAP-1 molecules touch the K^+ ion not at its "equator" but at ~30° angle from the "north." Such an arrangement is a compromise of attractions of the PAP-1 oxygens to the K^+ ion, repulsions between the PAP-1 oxygens, and the implicit-solvent tendency to maximize the solvent-exposed surface of the K^+ ion. These results further confirm the predictive power of Monte Carlo-minimizations with implicit solvent and explicit metal ions, which have been demonstrated in simulations of Ca^{2+} binding to proteins (Cheng and Zhorov, 2010).

Probing of the Channel-Ligand Stoichiometry. The Hill coefficient of 2 determined for PAP-1 with a 10-concentration dose-concentration curve (Schmitz et al., 2005) for approximately 50 very closely related psoralens (Vennekamp et al., 2004; Schmitz et al., 2005; Bodendiek et al., 2009) and approximately 70 structurally related khellinones (Baell et al., 2004; Harvey et al., 2006) by whole-cell patch-clamp experiments unambiguously demonstrates that more than one cationophilic molecule binds simultaneously to one Kv1.3 channel. However, this Hill coefficient does not rule out the

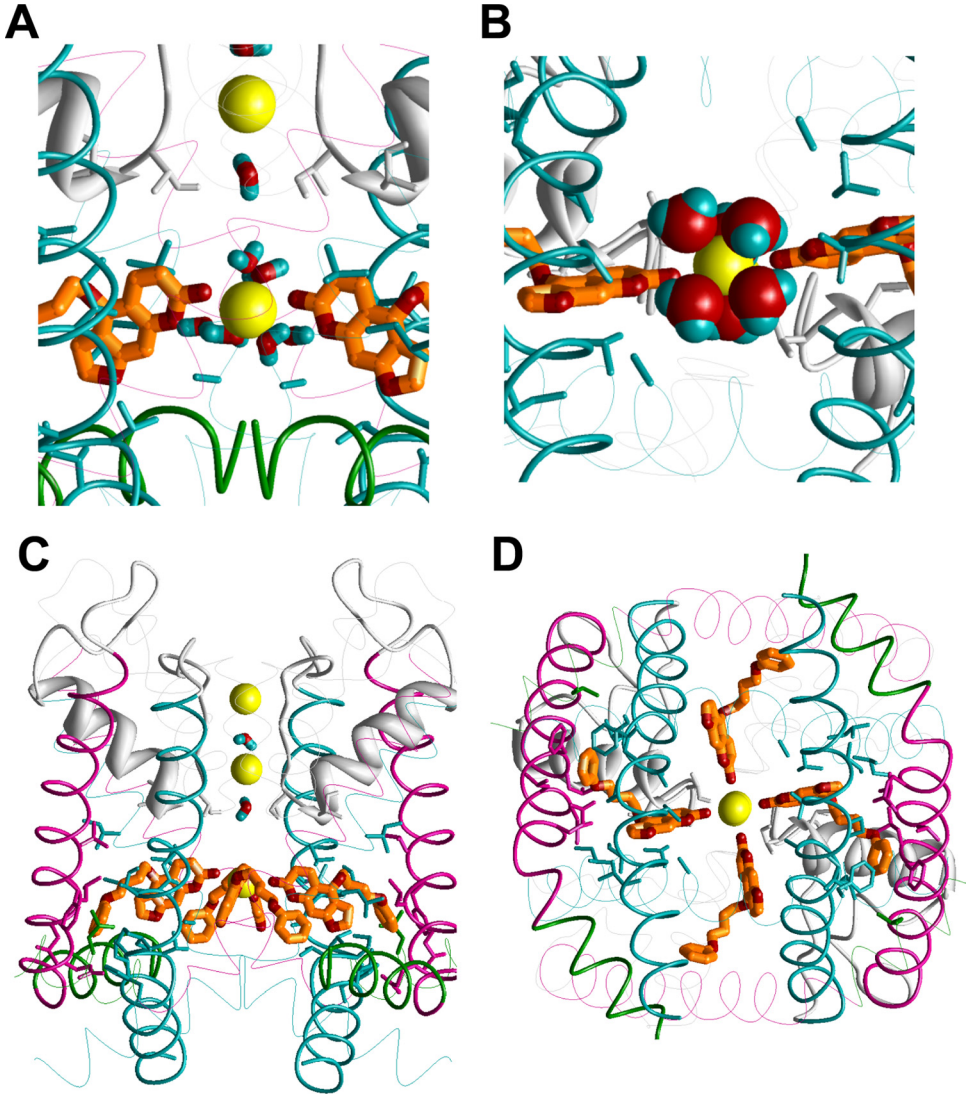

Fig. 5. A K^+ ion in the cavity center is attractive for PAP-1 and water molecules. Side (A) and cytoplasmic (B) views at Kv1.3 with two PAP-1 and six water molecules coordinating the K^+ ion. The water molecules at the cytoplasmic hemisphere of the K^+ ion donate H-bonds to the PAP-1 ether oxygens. Side (C) and cytoplasmic (D) views of the model with four PAP-1 molecules. See text for further details.

possibility that more than two PAP-1 ligands could bind to the channel. We therefore asked whether our Kv1.3 model could accommodate more than two PAP-1 ligands. Because docking of two PAP-1 molecules practically did not deform the backbones of the channel protein, the two remaining ligand-vacant subunit interfaces have as much space as any subunit interface in the ligand-free channel. To illustrate this, we placed two more PAP-1 ligands into the model shown in Fig. 4, MC-minimized the model with four ligands, and arrived at the structure shown in Fig. 5, C and D. All four PAP-1 molecules fit snugly into the channel, do not repel each other, have ligand-channel energies as favorable as in the complex with two PAP-1 molecules, and jointly coordinate the K^+ ion in the cavity center. These calculations suggest that binding of four ligands is thermodynamically possible. Whether the binding is kinetically possible is unknown. Indeed, binding of the third and fourth PAP-1 molecules might require too much time because the pore cavity occupied by two ligands looks less accessible for the newcomers, resulting in higher free-energy association barriers. One feasible approach to further probe the stoichiometry of the PAP-1:Kv1.3 interaction in future experiments would be to perform equilibrium binding assays with radiolabeled PAP-1. Similar studies were performed previously with a radiolabeled disubstituted cyclohexyl derivative and elegantly demonstrated that this class of molecules binds to two identical binding sites on the Kv1.3 channel (Schmalhofer et al., 2003).

Experimental Testing of the Molecular Model. To experimentally test the PAP-1 binding site model, we performed an alanine scan of 41 residues (Fig. 6 and Supplemental Table S1) in and around the predicted receptor (native alanines were mutated to serines). Positions at which alanine substitutions significantly slowed C-type inactivation or produced nonfunctional channels were mutated to more conservative amino acids. A total of 58 point mutants were generated. Because mutations can change PAP-1 affinity directly, allosterically (e.g., via slowing C-type inactivation), or by both mechanisms, we measured the half-activation voltage, activation and inactivation time constants, and degree of cumulative inactivation of each mutant before determining the PAP-1 IC_{50} for current inhibition. Mutant channels with significantly slower inactivation and/or reduced cumulative use-dependence (colored green in Fig. 6 and Supplemental Table S1) were excluded from the analysis, and only mutants demonstrating biophysical properties similar to the wild-type Kv1.3 channel were considered to affect PAP-1 potency directly rather than allosterically. Excluding mutants with altered inactivation and use-dependence was particularly important for our study, because a delay or loss of C-type inactivation reduces PAP-1 potency (Schmitz et al., 2005) and would have produced false-positive results.

The predicted PAP-1 receptor comprises 19 residues in L45, S5, S6, and the P-loop segments (Fig. 4, A, D, and E). Substitutions of 15 of these residues produced functional channels, whereas substitutions of four residues did not express. Substitutions of 12 WT residues in the predicted PAP-1 receptor (E^{o6}, L^{o10}, F^{o13}, T^{p48}, I^{i12}, V^{i15}, L^{i16}, T^{i17}, I^{i18}, L^{i20}, V^{i22}, and V^{i25}) significantly changed PAP-1 potency (Figs. 4A and 6; Supplemental Table S1), and substitutions of only four of these residues ($L^{o10}A$, $I^{i12}A$, $V^{i22}A$, and $I^{i25}A$) demonstrated a significant delay of C-type inactivation suggesting structural changes. Two mutants ($E^{o6}A$, $F^{o13}Y$) showed significantly increased PAP-1 sensitivity, whereas the remaining six mutants ($T^{p47}S$, $V^{i15}A$, $L^{i16}A$, $T^{i17}A$, $I^{i18}L$, and $L^{i20}I$) showed decreased sensitivity. Representative cur-

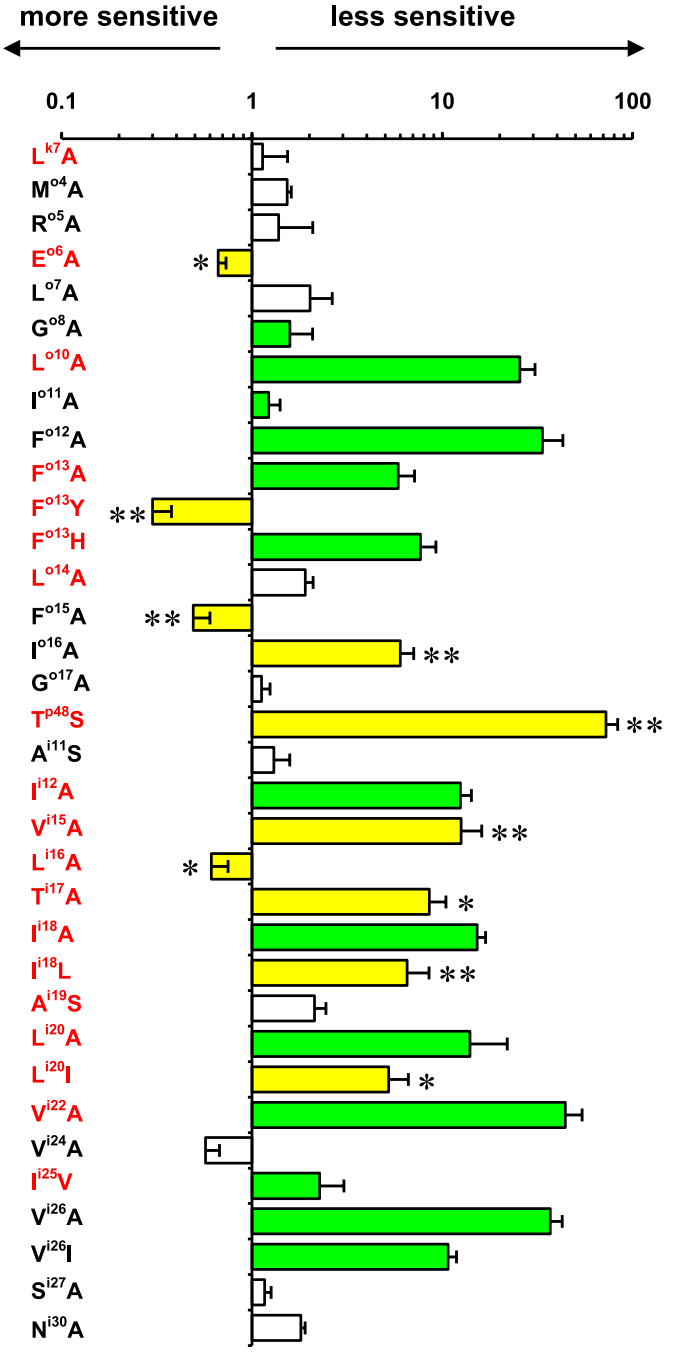

Fig. 6. Comparison of PAP-1 potencies on Kv1.3 mutants. The ratio of the IC_{50} of the mutant channel to the IC_{50} of the wild-type channel at corresponding holding potentials is plotted. Please note the logarithmic scale. Error bars indicate standard deviations calculated using propagation of uncertainty rules (*, $p < 0.05$, **, $p < 0.01$, two-tailed unpaired Student's t test). Yellow bars indicate mutants with significant changes in PAP-1 potency without significant delays in C-type inactivation. White bars indicate mutants without delayed C-type inactivation and no significant changes in PAP-1 potency ($p > 0.05$). Green bars indicate mutations that significantly delayed C-type inactivation (with or without significant changes in PAP-1 potency) and were therefore excluded from the analysis. Mutants whose respective wild-type residues are within 5 Å from the PAP-1 ligands in the model (Fig. 4) are highlighted in red.

rent traces of the mutants that produced the most drastic changes in PAP-1 potency are shown in Fig. 7.

As a negative control, we also mutated 14 residues around the predicted receptor, which were not predicted to be involved in PAP-1 binding. Mutations $M^{o4}A$, $R^{o5}A$, $L^{o7}A$, $G^{o17}A$, $A^{i11}S$, and $V^{i24}A$ had little effect on PAP-1 potency and C-type inactivation. Mutations $G^{o8}A$, $I^{o11}A$, $F^{o12}A$, $V^{i26}A$, $S^{i27}A$, and $N^{i30}A$ slowed C-type inactivation. Only mutations $F^{o15}A$ and $I^{o16}A$ changed PAP-1 sensitivity without significantly delaying C-type inactivation. Both positions are immediately C-terminal to the predicted PAP-1-sensing residues (Fig. 3A) and might therefore exert "neighboring" effects. Taken together, the results of the mutagenesis experiments support the molecular model by correctly predicting 8 of 11 PAP-1-sensing residues, which are analyzable because the biophysical properties of the respective point mutants suggest no significant structural changes in the ligand-free channel.

Because our model suggested that two (or possibly up to four) PAP-1 molecules chelate a K^+ ion in the inner pore of Kv1.3, we wondered whether changing K^+ concentration or substitution of the permeating ion would affect PAP-1 potency. Unfortunately, increasing extracellular K^+ from 4.5 to 40 or 80 mM at a holding potential of −100 mV significantly affected C-type inactivation and reduced use-dependence (data not shown), making it impossible to obtain meaningful interpretations from changes in PAP-1 affinity under these conditions. Reducing intracellular K^+ from 160 to 80 or 40 mM at a holding potential of −100 mV did not affect inactivation and use-dependence and reduced the IC_{50} of PAP-1 from 3.7 ± 0.4 to 8.8 ± 2.8 or 6.7 nM. Although these changes were not statistically significant, their trend might suggest that less K^+ is available for complex formation at site T5.

In addition to K^+, Kv1.3 is permeable to Rb^+ (0.77), NH_4^+ (0.1), and Cs^+ (0.02), with numbers in brackets indicating the permeability relative to that of K^+ (Cahalan et al., 1985). We decided not to substitute Cs^+ for K^+ because of the extremely low conductance with Cs^+. However, we tried substitutions of internal K^+ with NH_4^+ or Rb^+. Although NH^+ substitution resulted in a dramatic acceleration of inactivation and insufficient recovery from inactivation, substitution of $[K^+]_i$ with 160 mM Rb^+ did not affect inactivation properties (data not shown) and did not result in a significant change in the IC_{50} of PAP-1 (2 nM at −80 mV), presumably because of the great similarity between Rb^+ and K^+. We further substituted K^+ with Rb^+ in the model shown in Fig. 5, A and B, MC minimized the complex of Kv1.3 with the tripartite blocker and six explicit water molecules and found the square-antiprism coordination geometry of Rb^+ to be very similar to that of K^+. The predicted oxygen-to-Rb^+ distances were ~ 0.1 to 0.2 Å longer than the respective oxygen-to-K^+ distances, the energy contribution of Rb^+_{T5} to the PAP-1 binding energy was ~0.1 kcal/mol lower (more negative) than that of K^+_{T5} (Supplemental Table S4), whereas the interaction energy between PAP-1 and the channel amino acids (Supplemental Table S4) practically did not change (data not shown). These calculations support our experimental observation and are in agreement with experimental data on Rb^+

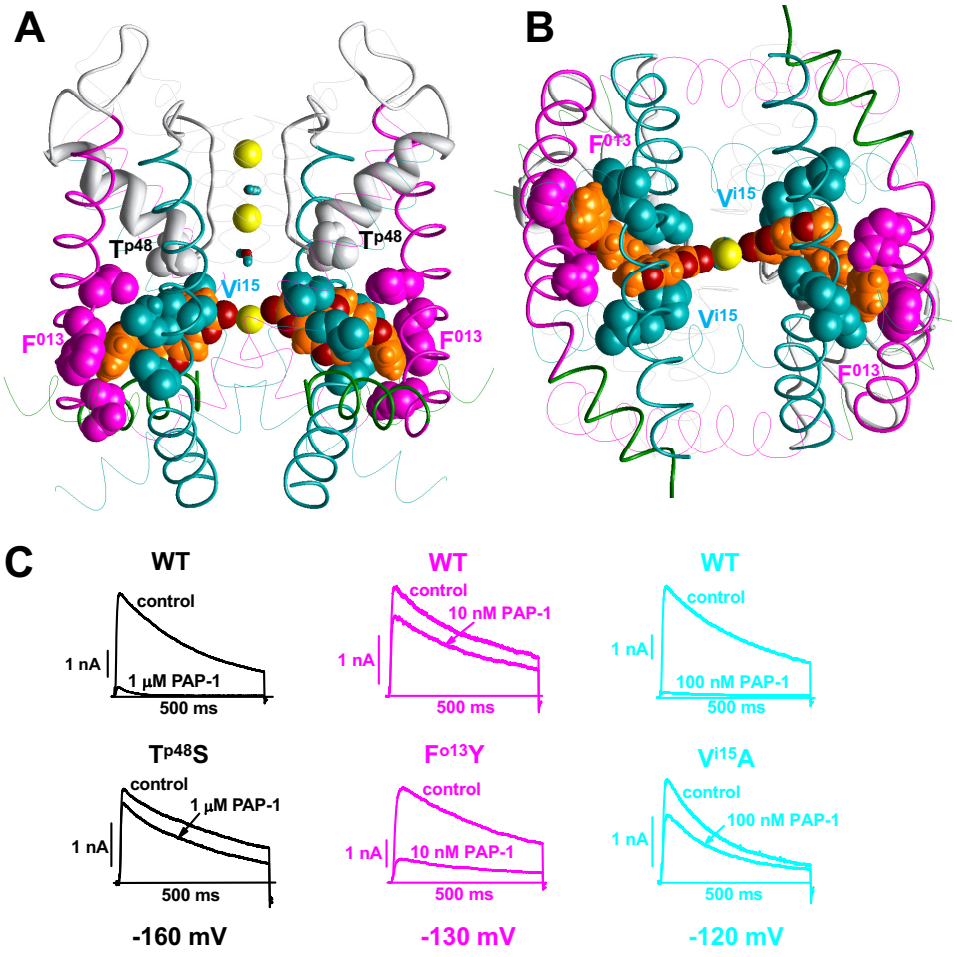

Fig. 7. Side (A) and cytoplasmic (B) views of Kv1.3 blocked by the tripartite complex PAP-1:K^+:PAP-1. Of 12 residues whose mutations changed PAP-1 potency with little effect on inactivation (Supplemental Table S1), 10 are space-filled. These are T^{p48} at the turns of the P-loops (light gray); E^{o6}, F^{o13}, and L^{o14} in S5s (magenta); and V^{i15}, L^{i16}, T^{i17}, I^{i18}, and L^{i20} in S6s (cyan). These residues constitute most of the PAP-1 binding site (compare with Fig. 4 that shows all residues within 5 Å from the ligands). C, representative current traces for WT (top row) and mutants at specific holding potentials. The traces are colored like the respective WT residues in A and B. Note that PAP-1 potency changes with the holding potential because of the voltage-dependence of block (IC_{50} at −100 mV = 4 nM; IC_{50} at −130 mV = 13 nM; IC_{50} at −160 mV = 140 nM).

hydration (D'Angelo and Persson, 2004) and molecular dynamics simulations of a potassium channel with Rb^+ as the current-carrying cation (Domene and Sansom, 2003).

Discussion

Here we used electrophysiology, structure-activity studies, molecular modeling, and site-directed mutagenesis to predict the PAP-1 binding site on the lymphocyte Kv1.3 channel. Based on the observation that PAP-1 competes with known pore blockers such as internal TEA and verapamil we assumed that PAP-1 is an inner pore blocker. We further analyzed structure-activity data that the PAP-1 coumarin ring is essential for activity and that block by the uncharged lipophilic PAP-1 molecules is voltage-dependent and arrived at the hypothesis that PAP-1 binds to a K^+ ion below the selectivity filter of the Kv1.3 channel. This hypothesis fits our concept proposed previously that the permeating ions in cation channels may directly interact with electron-rich groups of pore-binding ligands. The hypothesis allowed us to define distance constraints that substantially decreased the search space for the PAP-1 receptor during molecular modeling. Without these knowledge-based constraints, it would not have been feasible to predict the complex computationally by hands-free docking of so flexible ligand as PAP-1 into the flexible Kv1.3 model. The molecular model was then used to guide the focused mapping of the PAP-1 receptor through mutagenesis and electrophysiology. The agreement between the atomistic model and the results of the experiments demonstrates the advantages of combining computational and experimental approaches.

Our study proposes a K^+ ion to be an indispensable component of the PAP-1 receptor and explains our previous failure to design a potent Kv1.3 blocker that lacks the coumarin ring system (Bodendiek et al., 2009), which we had wanted to eliminate because this structural element can potentially act as a Michael acceptor and cause liver toxicity by reacting with glutathione. When attaching the 4-phenoxybutoxy side chain of PAP-1 to other planar heterocyclic systems, we had observed that phenoxyalkoxypsoralen-type Kv1.3 blockers have a very steep structure-activity relationship and that the coumarin system cannot be replaced (Bodendiek et al., 2009). Our model explains these structure-activity findings and the Hill coefficient of 2 and shows that the coumarin rings of two PAP-1 molecules are located in the inner pore but do not block ion permeation per se. It is the K^+ ion between the two PAP-1 molecules that blocks the permeation pathway. Only one oxygen atom of each PAP-1 molecule interacts with the K^+ ion. In the open channel, incoming K^+ ions would displace the ion and probably destroy the tripartite blocking complex. However, because ion flow is stopped in the inactivated state, the tripartite blocker would be more stable under these conditions, explaining the preferential effect of PAP-1 on the C-type-inactivated state of Kv1.3 (Schmitz et al., 2005).

Despite the relatively large molecular weight of PAP-1 (350 Da), two or even four PAP-1 molecules are easily accommodated in the inner-pore region of the channel (Figs. 4 and 7). Only the parts of the coumarin rings that contain the carbonyl and ether oxygens are exposed to the central cavity, in which they interact with the K^+ ion at the focus of the P-helices and ordered water molecules in the K^+ solvation shell, as well as with the pore-facing residues T^{p48}, V^{i15}, and I^{i18}, whereas the long, flexible butoxyphenyl moieties wrap

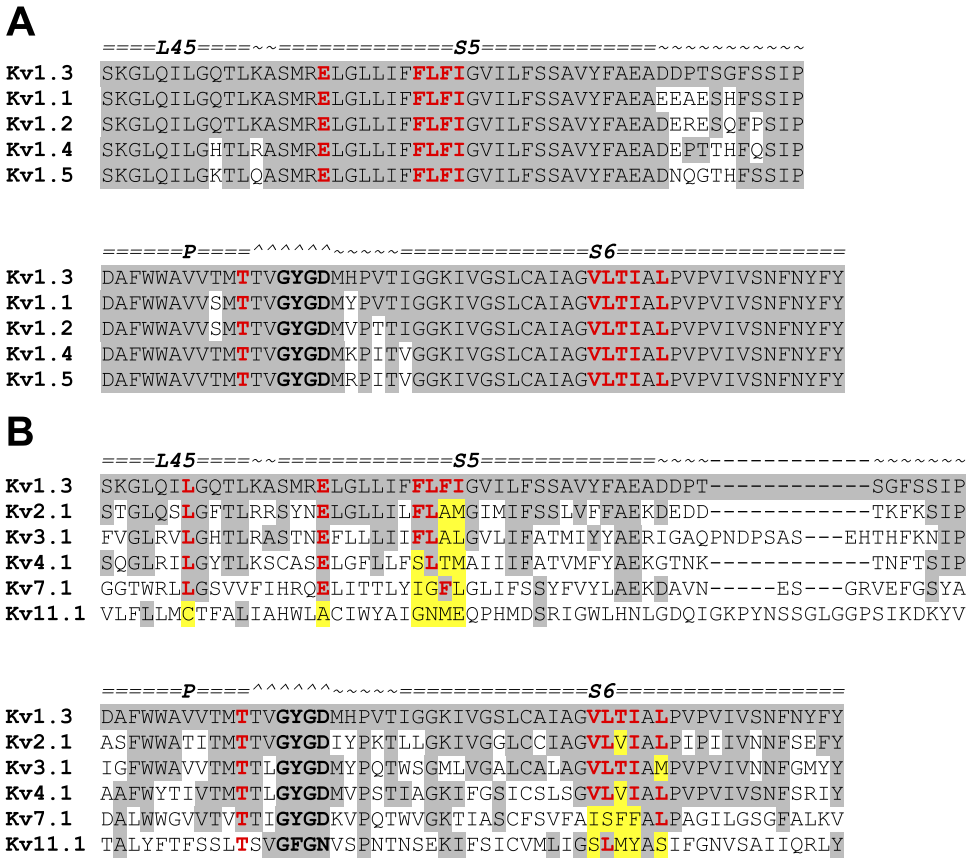

Fig. 8. Sequence alignments of the pore-forming domains of Kv1.3 with Kv1 and non-Kv1 channels. Experimentally confirmed PAP-1-sensing residues in Kv1.3 and same-type residues in matching positions of other channels are highlighted in red. A, alignment of Kv1.3 with human Kv1 channels. The sequences are identical with Kv1.3 in the PAP-1-sensing regions, and the main differences are in the extracellular linkers S5-P and P-S6, in which mutations are known to affect the kinetics of C-type inactivation. This may explain the 23- to 125-fold selectivity of PAP-1 for Kv1.3 over other Kv1 channels. B, alignment of Kv1.3 with representative members of the Kv2, Kv3, Kv4, Kv7, and Kv10 family. Residues that differ from the PAP-1-sensing residues in Kv1.3 are shown on yellow background. Non-Kv1 sequences differ from Kv1.3 in two or more positions in which Kv1.3 has PAP-1-sensing residues. In addition, many residues in flanking positions to PAP-1-sensing residues in Kv1.3 are also different in non-Kv1 channels versus Kv1.3. This may explain the thousand-fold selectivity of PAP-1 for Kv1.3 over non-Kv1 channels.

around the inner helices and fit nicely between helices S5 and S6 (Fig. 7). Interestingly, this space seems to be able to accommodate PAP-1 derivatives as large as AS-85 (Fig. 3), which bears an additional phenoxy-substituent on the phenyl ring (Vennekamp et al., 2004; Schmitz et al., 2005; Boden diek et al., 2009).

The inner pore of Kv channels has long been known as a target for small molecules, and many classic Kv channel blockers such as TEA, 4-aminopyridine, verapamil, and D-tubocurarine have been shown to bind to this region (Wulff and Zhorov, 2008). Besides the K^+ ion, the receptor for a single PAP-1 molecule involves four loci, which contain experimentally confirmed PAP-1-sensing residues from five segments, namely, three of the four S6s, S5, and the P-loop. The mutation that produces the largest change in PAP-1 affinity (70-fold) is $T^{p48}S$ at the bottom of the pore loop in locus I (Fig. 7). This particular position has been described previously to be involved in the binding of the antiarrhythmic drug (+)-*N*-[1′-(6-cyano-1,2,3,4-tetrahydro-2(*R*)-naphthalenyl)-3,4-dihydro-4(*R*)-hydroxyspiro(2*H*-1-benzopyran-2,4′-piperidin)-6-yl]methanesulfonamide] monohydrochloride (MK-499) to the human *ether-a-go-go*-related gene channel (Mitcheson et al., 2000) and of Kv1.5 channel blockers (Decher et al., 2004, 2006). The neighboring T^{p49} at the top of locus I has also been identified as a ligand-sensing residue in the calcium-activated K^+ channel KCa3.1, in which it determines sensitivity to the triarylmethanes clotrimazole and 1-[(2-chlorophenyl)diphenylmethyl]-1*H*-pyrazole (TRAM-34) and arachidonic acid (Wulff et al., 2001; Hamilton et al., 2003). Mutation of T^{p49} to alanine in Kv1.3 did not produce functional channels in our study (Supplemental Table S1), but the residue binds a water molecule at site four of the selectivity filter in our model and was also predicted to contribute to the PAP-1 receptor (Fig. 4 and Supplemental Table S2). The most important determinant of the PAP-1 receptor in our model is a K^+ ion, which is stabilized by electrostatic interactions with the C-termini of P-helixes. This region at the focus of the P-helices constitutes a common and attractive binding site for both organic and inorganic cations (Wulff and Zhorov, 2008).

In the voltage-gated L-type Ca^{2+} channel, dihydropyridine and benzothiazepine ligands were proposed to bind in the domain interface involving helices 3S5, 3S6, and 4S6 (Hockerman et al., 1997; Tikhonov and Zhorov, 2008, 2009), an equivalent of locus II in the PAP-1 receptor (Supplemental Fig. S1). In the insect Na^+ channel, pyrethroid agonists bind between helices 3S6, 2S5, and 2L45 (O'Reilly et al., 2006), an equivalent of locus IV of the PAP-1 receptor (Supplemental Table S2 and Fig. S1). However, we are not aware of other studies of P-loop channels that describe ligand binding between helices S5 and S6 of the same subunit/domain, an equivalent of locus III in the PAP-1 receptor. Mutations of residue T^{i17} in this locus reduce PAP-1 affinity by 9-fold (Supplemental Table S1).

The PAP-1 binding site model provides a rational explanation for the experimentally observed Hill coefficient of 2, the compound's voltage-dependence of block and its selectivity for Kv1.3 over Kv2, Kv3, Kv4, Kv7, and Kv11 channels, which all show sequence differences in positions in which Kv1.3 has PAP-1-sensing residues (Fig. 8). However, our model, which is based on the open Kv1.2 channel structure, does not explain the 23- to 125-fold selectivity of PAP-1 for Kv1.3 over the closely related Kv1-family channels Kv1.1, Kv1.2, Kv.1.4, Kv1.5, Kv1.6, and Kv1.7, which are identical in positions in which Kv1.3 has PAP-1-sensing residues (Fig. 8). This selectivity therefore must be caused by the preferential affinity of PAP-1 to the C-type inactivated state. Indeed, removal of C-type inactivation either by mutation of H^{p56}, a residue in the extracellular P–S6 linker, which is not involved in PAP-1 binding in our model, or by high extracellular K^+ concentration reduces PAP-1 potency in Kv1.3 approximately 20-fold, to the level of Kv1.5 (Schmitz et al., 2005). Continued K^+ flux in the absence of C-type inactivation would destabilize the tripartite PAP-1:K^+-PAP-1 complex in the channel pore, whereas cessation of K^+-flux after C-type inactivation probably stabilizes the complex. In conclusion, our study provides a rationale for the intriguing chemical diversity of drugs targeting the inner-pore region of Kv channels, presents a new concept for Kv channels block by cationophilic ligands, and reveals a new ligand-binding locus in the S5/S6 interface.

Acknowledgments

We thank Dr. Jerry L. Dallas for help with the 800-MHz ^{13}C NMR experiments.

References

Aiyar J, Nguyen AN, Chandy KG, and Grissmer S (1994) The P-region and S6 of Kv3.1 contribute to the formation of the ion conduction pathway. *Biophys J* **67:**2261–2264.
Armstrong CM (1971) Interaction of tetraethylammonium ion derivatives with the potassium channels of giant axons. *J Gen Physiol* **58:**413–437.
Armstrong CM and Binstock L (1965) Anomalous rectification in the squid giant axon injected with tetraethylammonium chloride. *J Gen Physiol* **48:**859–872.
Azam P, Sankaranarayanan A, Homerick D, Griffey S, and Wulff H (2007) Targeting effector memory T cells with the small molecule Kv1.3 blocker PAP-1 suppresses allergic contact dermatitis. *J Invest Dermatol* **127:**1419–1429.
Baell JB, Gable RW, Harvey AJ, Toovey N, Herzog T, Hänsel W, and Wulff H (2004) Khellinone derivatives as blockers of the voltage-gated potassium channel Kv1.3: synthesis and immunosuppressive activity. *J Med Chem* **47:**2326–2336.
Beeton C, Wulff H, Standifer NE, Azam P, Mullen KM, Pennington MW, Kolski-Andreaco A, Wei E, Grino A, Counts DR, et al. (2006) Kv1.3 channels are a therapeutic target for T cell-mediated autoimmune diseases. *Proc Natl Acad Sci USA* **103:**17414–17419.
Bodendiek SB, Mahieux C, Hänsel W, and Wulff H (2009) 4-Phenoxybutoxy-substituted heterocycles–a structure-activity relationship study of blockers of the lymphocyte potassium channel Kv1.3. *Eur J Med Chem* **44:**1838–1852.
Brock MW, Mathes C, and Gilly WF (2001) Selective open-channel block of Shaker (Kv1) potassium channels by s-nitrosodithiothreitol (SNDTT). *J Gen Physiol* **118:** 113–134.
Brooks CL, Pettitt BM, and Karplus M (1985) Structural and energetic effects of truncating long ranged interactions in ionic polar fluids. *J Chem Phys* **83:**5897–5908.
Bruhova I and Zhorov BS (2007) Monte Carlo-energy minimization of correolide in the Kv1.3 channel: possible role of potassium ion in ligand-receptor interactions. *BMC Struct Biol* **7:**5.
Cahalan MD, Chandy KG, DeCoursey TE, and Gupta S (1985) A voltage-gated potassium channel in human T lymphocytes. *J Physiol* **358:**197–237.
Chandy KG, Wulff H, Beeton C, Pennington M, Gutman GA, and Cahalan MD (2004) K^+ channels as targets for specific immunomodulation. *Trends Pharmacol Sci* **25:**280–289.
Cheng RC, Tikhonov DB, and Zhorov BS (2009) Structural model for phenylalkylamine binding to L-type calcium channels. *J Biol Chem* **284:**28332–28342.
Cheng RC and Zhorov BS (2010) Docking of calcium ions in proteins with flexible side chains and deformable backbones. *Eur Biophys J* **39:**825–838.
D'Angelo P and Persson I (2004) Structure of the hydrated and dimethyl sulfoxide solvated rubidium ions in solution. *Inorg Chem* **43:**3543–3549.
Decher N, Kumar P, Gonzalez T, Pirard B, and Sanguinetti MC (2006) Binding site of a novel Kv1.5 blocker: a "foot in the door" against atrial fibrillation. *Mol Pharmacol* **70:**1204–1211.
Decher N, Pirard B, Bundis F, Peukert S, Baringhaus KH, Busch AE, Steinmeyer K, and Sanguinetti MC (2004) Molecular basis for Kv1.5 channel block: conservation of drug binding sites among voltage-gated K^+ channels. *J Biol Chem* **279:**394–400.
del Camino D, Holmgren M, Liu Y, and Yellen G (2000) Blocker protection in the pore of a voltage-gated K^+ channel and its structural implications. *Nature* **403:**321–325.
Dewar MJ, Zoebisch EG, Healy EF, and Stewart JJ (1985) AM1: a new general purpose quantum mechanical model. *J Am Chem Soc* **107:**3902–3907.
Domene C and Sansom MS (2003) Potassium channel, ions, and water: simulation studies based on the high resolution X-ray structure of KcsA. *Biophys J* **85:**2787–2800.
Dreker T and Grissmer S (2005) Investigation of the phenylalkylamine binding site

in hKv1.3 (H399T), a mutant with a reduced C-type inactivated state. *Mol Pharmacol* **68:**966–973.
Faraldo-Gómez JD, Kutluay E, Jogini V, Zhao Y, Heginbotham L, and Roux B (2007) Mechanism of intracellular block of the KcsA K^+ channel by tetrabutylammonium: insights from X-ray crystallography, electrophysiology and replica-exchange molecular dynamics simulations. *J Mol Biol* **365:**649–662.
Garden DP and Zhorov BS (2010) Docking flexible ligands in proteins with a solvent exposure- and distance-dependent dielectric function. *J Comput Aided Mol Des* **24:**91–105.
Hamilton KL, Syme CA, and Devor DC (2003) Molecular localization of the inhibitory arachidonic acid binding site to the pore of hIK1. *J Biol Chem* **278:**16690–16697.
Harvey AJ, Baell JB, Toovey N, Homerick D, and Wulff H (2006) A new class of blockers of the voltage-gated potassium channel Kv1.3 via modification of the 4- or 7-position of khellinone. *J Med Chem* **49:**1433–1441.
Hazel JP and Collin RL (1972) The crystal structure of potassium *O,O*-dibenzylphosphorodithioate $KS_2P(O\text{-}CH_2\text{-}C_6H_5)_2$. *Acta Crystallogr B* **28:**2279–2287.
Hockerman GH, Peterson BZ, Johnson BD, and Catterall WA (1997) Molecular determinants of drug binding and action on L-type calcium channels. *Annu Rev Pharmacol Toxicol* **37:**361–396.
Lazaridis T and Karplus M (1999) Effective energy function for proteins in solution. *Proteins* **35:**133–152.
Lenaeus MJ, Vamvouka M, Focia PJ, and Gross A (2005) Structural basis of TEA blockade in a model potassium channel. *Nat Struct Mol Biol* **12:**454–459.
Li Z and Scheraga HA (1987) Monte Carlo-minimization approach to the multiple-minima problem in protein folding. *Proc Natl Acad Sci USA* **84:**6611–6615.
Long SB, Campbell EB, and Mackinnon R (2005) Crystal structure of a mammalian voltage-dependent Shaker family K^+ channel. *Science* **309:**897–903.
Meeder T and Ulbricht W (1987) Action of benzocaine on sodium channels of frog nodes of Ranvier treated with chloramine-T. *Pflugers Arch* **409:**265–273.
Mitcheson JS, Chen J, Lin M, Culberson C, and Sanguinetti MC (2000) A structural basis for drug-induced long QT syndrome. *Proc Natl Acad Sci USA* **97:**12329–12333.
O'Reilly AO, Khambay BP, Williamson MS, Field LM, Wallace BA, and Davies TG (2006) Modelling insecticide-binding sites in the voltage-gated sodium channel. *Biochem J* **396:**255–263.
Panyi G, Sheng Z, and Deutsch C (1995) C-type inactivation of a voltage-gated K^+ channel occurs by a cooperative mechanism. *Biophys J* **69:**896–903.
Rauer H and Grissmer S (1996) Evidence for an internal phenylalkylamine action on the voltage-gated potassium channel Kv1.3. *Mol Pharmacol* **50:**1625–1634.
Sanguinetti MC and Tristani-Firouzi M (2006) hERG potassium channels and cardiac arrhythmia. *Nature* **440:**463–469.
Schmalhofer WA, Bao J, McManus OB, Green B, Matyskiela M, Wunderler D, Bugianesi RM, Felix JP, Hanner M, Linde-Arias AR, et al. (2002) Identification of a new class of inhibitors of the voltage-gated potassium channel, Kv1.3, with immunosuppressant properties. *Biochemistry* **41:**7781–7794.
Schmalhofer WA, Slaughter RS, Matyskiela M, Felix JP, Tang YS, Rupprecht K, Kaczorowski GJ, and Garcia ML (2003) Di-substituted cyclohexyl derivatives bind to two identical sites with positive cooperativity on the voltage-gated potassium channel, K(v)1.3. *Biochemistry* **42:**4733–4743.
Schmitz A, Sankaranarayanan A, Azam P, Schmidt-Lassen K, Homerick D, Hänsel W, and Wulff H (2005) Design of PAP-1, a selective small molecule Kv1.3 blocker, for the suppression of effector memory T cells in autoimmune diseases. *Mol Pharmacol* **68:**1254–1270.
Sieler J, Beyer F, Hoyer E, Andersen L and Lindqvist O (1985) Trithione- and isotrithionedithiolate. A new class of unsaturated 1,2-dithiolates. IV. The crystal structure of dipotassium-1,2-dithiole-3-thion-4,5-dithiolate, $K_2C_3S_5$. *Acta Chem Scand A* **39:**153–156.
Tikhonov DB, Bruhova I, and Zhorov BS (2006) Atomic determinants of state-dependent block of sodium channels by charged local anesthetics and benzocaine. *FEBS Lett* **580:**6027–6032.
Tikhonov DB and Zhorov BS (2007) Sodium channels: ionic model of slow inactivation and state-dependent drug binding. *Biophys J* **93:**1557–1570.
Tikhonov DB and Zhorov BS (2008) Molecular modeling of benzothiazepine binding in the L-type calcium channel. *J Biol Chem* **283:**17594–17604.
Tikhonov DB and Zhorov BS (2009) Structural model for dihydropyridine binding to L-type calcium channels. *J Biol Chem* **284:**19006–19017.
Vennekamp J, Wulff H, Beeton C, Calabresi PA, Grissmer S, Hänsel W, and Chandy KG (2004) Kv1.3-blocking 5-phenylalkoxypsoralens: a new class of immunomodulators. *Mol Pharmacol* **65:**1364–1374.
Weiner SJ, Kollman PA, Case DA, Singh UC, and Chio C (1984) A new force field for molecular mechanical simulation of nucleic acids and proteins. *J Am Chem Soc* **106:**765–784.
Weiner SJ, Kollman PA, Nguen DT, and Case DA (1986) An all atom force field for simulations of proteins and nucleic acids. *J Comput Chem* **7:**230–252.
Wulff H, Gutman GA, Cahalan MD, and Chandy KG (2001) Delineation of the clotrimazole/TRAM-34 binding site on the intermediate conductance calcium-activated potassium channel, IKCa1. *J Biol Chem* **276:**32040–32045.
Wulff H and Pennington M (2007) Targeting effector memory T-cells with Kv1.3 blockers. *Curr Opin Drug Discov Devel* **10:**438–445.
Wulff H and Zhorov BS (2008) K^+ channel modulators for the treatment of neurological disorders and autoimmune diseases. *Chem Rev* **108:**1744–1773.
Zhorov BS (1981) Vector method for calculating derivatives of energy of atom-atom interactions of complex molecules according to generalized coordinates. *J Struct Chem* **22:**4–8.
Zhorov BS (1983) Vector method for calculating derivatives of the energy deformation of valence angles and torsion energy of complex molecules according to generalized coordinates. *J Struct Chem* **23:**649–655.
Zhou M, Morais-Cabral JH, Mann S, and MacKinnon R (2001a) Potassium channel receptor site for the inactivation gate and quaternary amine inhibitors. *Nature* **411:**657–661.
Zhou P, Tian F, Lv F, and Shang Z (2009) Geometric characteristics of hydrogen bonds involving sulfur atoms in proteins. *Proteins* **76:**151–163.
Zhou Y, Morais-Cabral JH, Kaufman A, and MacKinnon R (2001b) Chemistry of ion coordination and hydration revealed by a K^+ channel-Fab complex at 2.0 A resolution. *Nature* **414:**43–48.

Address correspondence to: Dr. Boris S. Zhorov, Department of Biochemistry and Biomedical Sciences, McMaster University, Hamilton, ON, Canada. E-mail: zhorov@mcmaster.ca